(Received 23 August 2025, Accepted 22 September 2025, Scheduled 27 September 2025)

A Miniaturized Highly Isolated Two Port Triple Band-Notched UWB MIMO Antenna verified by Characteristic Mode Analysis

Haritha Thotakura[1], Rajesh Gogineni[2], K Srinivasa Rao[3], Chunduri Kiran Kumar[4], Rameshbabu Sadineni[5,*], and Sunitha Mandava[5]

[1]*Department of Electronics & Communication Engineering, PVP Siddhartha Institute of Technology, Vijayawada, India*
[2]*Department of Electronics & Communication Engineering, Dhanekula Institute of Engineering and Technology, Ganguru, India*
[3]*Department of Electronics & Communication Engineering, Andhra Loyola Institute of Engineering and Technology Vijayawada, India*
[4]*Department of CSA, Koneru Lakshmaiah Education Foundation, Vaddeswaram, AP, India*
[5]*Department of Electronics & Communication Engineering, RVR&JC College of Engineering, Guntur, India*

ABSTRACT: This article presents a compact highly isolated two-port ultra-wideband (UWB) multiple-input multiple-output (MIMO) antenna with triple band suppression features. The antenna measures $25 \times 39\,\text{mm}^2$ and comprises two orthogonally arranged microstrip-fed square radiators to achieve high inter-element isolation. A T-shaped and L-shaped stubs were incorporated into the ground plane to enhance isolation and broaden the impedance bandwidth. Triple band notches targeting Satellite C-band downlink (3.6–4.6 GHz), WLAN (4.9–5.5 GHz), and Wi-Fi 6E (6.1–6.7 GHz) are realized using three U-shaped slots introduced on each radiating element. The antenna's operation is analyzed through Characteristic Mode Analysis (CMA) by evaluating modal significance, characteristic angle, modal currents, and mode patterns. MIMO performance is validated using key diversity metrics, including envelope correlation coefficient (ECC), diversity gain (DG), total active reflection coefficient (TARC), channel capacity loss (CCL), multiplexing efficiency (ME), and group delay. Results demonstrate an impedance bandwidth exceeding 2.9–10.6 GHz UWB range, with 90% radiation efficiency, peak gain of 6.2 dBi, ECC below 0.02, and mutual coupling under -20 dB. These outcomes confirm the efficacy of the proposed antenna in achieving compactness and high performance for UWB MIMO applications.

1. INTRODUCTION

Ultra-wideband (UWB) systems have attracted substantial research interest due to their ability to support high data throughput, wide operational bandwidth, and cost-effective implementation [1]. Owing to their inherently low transmission power, UWB antennas are well suited for short-range wireless links, precise localization, tracking, and radar sensing applications [2, 3]. Numerous compact UWB antenna designs have been reported in literature [4, 5]. The integration of UWB with MIMO technology provides immunity to multipath fading [6]. In MIMO systems, however, the proximity of multiple antenna elements often results in mutual coupling, which degrades overall performance. To mitigate such coupling, various isolation enhancement approaches have been proposed, including neutralization lines [7], parasitic elements [8], and defected ground structures [9]. Another major design challenge for UWB antennas arises from electromagnetic interference caused by coexisting narrowband services. UWB coincides with several licensed systems, including WiMAX (3.2–3.8 GHz), C-band (3.6–4.6 GHz), INSAT (4.2–4.9 GHz), Wireless LAN (4.9–5.5 GHz), and X-band satellite links (7.7–8.4 GHz). Several designs achieving single, dual, and triple band notches have been reported. Examples include quasi-self-complementary MIMO antennas with WLAN rejection via slit loading [10], octagonal UWB-MIMO structures employing C-shaped slots for WLAN suppression and improved isolation [11], compact designs integrating band-reject filters for coupling reduction [12], and stepped-stub-based configurations offering both decoupling and band rejection [13]. Other works have demonstrated notching through T-shaped grooves with split-ring resonators [14], dual-notch generation using grooves and stubs [15], and pentagon-shaped radiators with dual-band suppression [16]. Studies in [17–31] present further variations with improved isolation and multi-band rejection. However, in many cases, residual gain and radiation efficiency at notch centers indicate incomplete suppression. Characteristic Mode Analysis (CMA), originally formulated by Garbacz in 1965 [32], provides a modal decomposition framework by identifying the natural resonant modes of a conducting structure. While most reported designs address single or dual notches, triple-band rejection remains less explored. Moreover, many existing solutions are physically large, limiting their suitability for portable applications.

This work presents a compact two-port UWB-MIMO antenna ($25 \times 39\,\text{mm}^2$) with -20 dB isolation achieved through ground-plane stubs and triple band suppression at 3.6–4.6 GHz, 4.9–5.5 GHz, and 6.1–6.7 GHz. The design integrates miniaturization, effective interference rejection, and strong isolation. Characteristic Mode Analysis (CMA) is employed to study modal significance, characteristic angle, and current distribu-

* Corresponding author: Ramesh Babu Sadineni (srbrvrece@gmail.com).

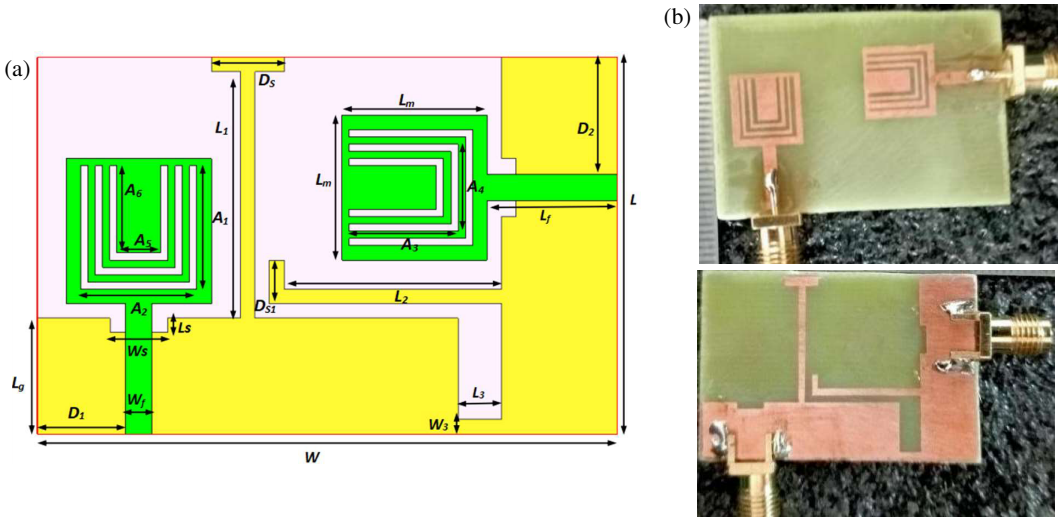

FIGURE 1. (a) Proposed band notched UWB MIMO antenna geometry. (b) Fabricated prototype (Top & Bottom view).

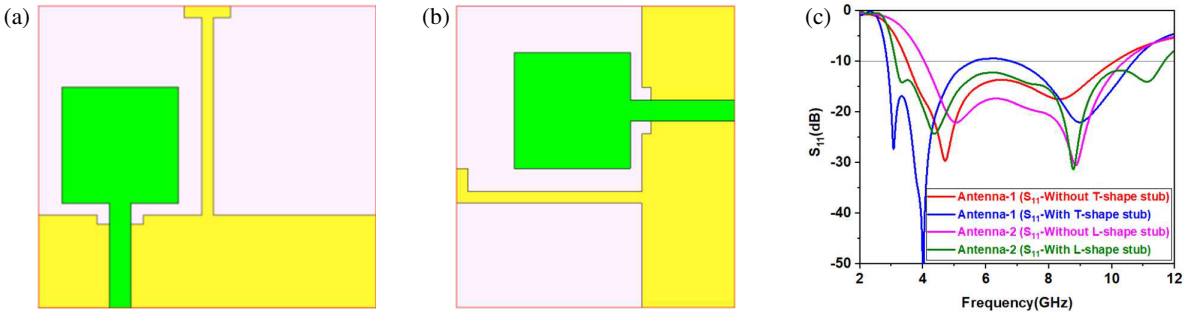

FIGURE 2. UWB antenna element. (a) Antenna-1. (b) Antenna-2. (c) Simulated S_{11}.

tions, offering insight into passband and notched-band behavior. MIMO performance is further evaluated in terms of ECC, DG, CCL, TARC, ME, and group delay.

2. ANTENNA DESIGN

The optimized geometry of the proposed band-notched UWB-MIMO antenna and its fabricated prototype model is depicted Fig. 1. It is implemented on an FR-4 substrate ($\varepsilon_r = 4.3$, thickness $= 1.6$ mm) with a compact footprint of $25 \times 39\,\text{mm}^2$. The design employs two identical square patches ($9 \times 9\,\text{mm}^2$) excited by $50\,\Omega$ microstrip lines ($1.7 \times 9\,\text{mm}^2$) and arranged orthogonally to enhance isolation by minimizing the overlap of surface currents and reducing near-field coupling between elements. Square geometry is adopted for its compactness and symmetry, enabling wide impedance bandwidth, stable radiation, and ease of MIMO integration. Partial ground planes (8 mm width, lengths of 29 mm and 25 mm) are etched on the backside, incorporating a 2.5×1 mm slot beneath each feed for impedance matching. Furthermore, T- and L-shaped stubs are integrated into the defected ground structure (DGS), which act as decoupling networks by interrupting current paths and redistributing surface currents. This combination of orthogonal patch placement and engineered ground stubs significantly suppresses mutual coupling, thereby achieving enhanced isolation over the entire UWB range.

Three U-shaped slots etched on radiator generate notches at 3.6–4.6 GHz (Satellite C-band), 4.9–5.5 GHz (WLAN), and 6.1–6.7 GHz (Wi-Fi 6E). The antenna is optimized in Computer Simulation Technology (CST) Microwave Studio to assess notch characteristics, impedance bandwidth, radiation performance, isolation, and peak gain. The optimized dimensional values are summarized in Table 1.

3. PROPOSED UWB MIMO ANTENNA EVOLUTION

3.1. Unit Antenna Element

The MIMO antenna under investigation comprises two UWB monopole components: Antenna-1 and Antenna-2, each equipped with dedicated ground planes and associated long stubs, as demonstrated in Fig. 2. To assess the impact of these stubs on bandwidth performance, a comparative simulation analysis was performed for the antenna elements both with and without their respective stubs.

From the simulation results illustrated in Fig. 2(c), it is evident that Antenna-1 without the T-shaped stub exhibits a lower -10 dB cutoff frequency around 3.4 GHz, which does not meet the UWB specification. However, introducing a T-stub gener-

TABLE 1. Optimized dimensional parameters (in mm).

L	Lm	Lf	$L1$	$L2$	$L3$	Ls	$D1$	Ds	$A1$	$A2$	$A5$
25	9	9	17	16	3	1	6.1	5	8.5	8	4.5
W	Lg	Wf	Ws	$Ds1$	$W3$	Ws	$D2$	Wg	$A3$	$A4$	$A6$
39	8	1.7	1	5	1	2.5	8.1	29	7.5	8	6.5

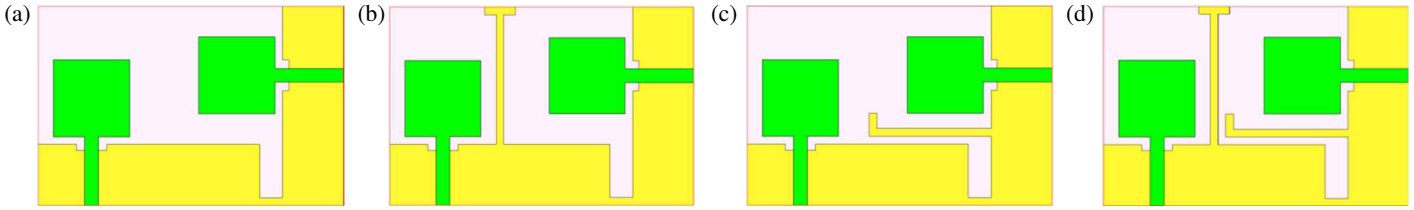

FIGURE 3. UWB MIMO Antenna evolution (without notches). (a) Antenna-3. (b) Antenna-4. (c) Antenna-5. (d) Antenna-6.

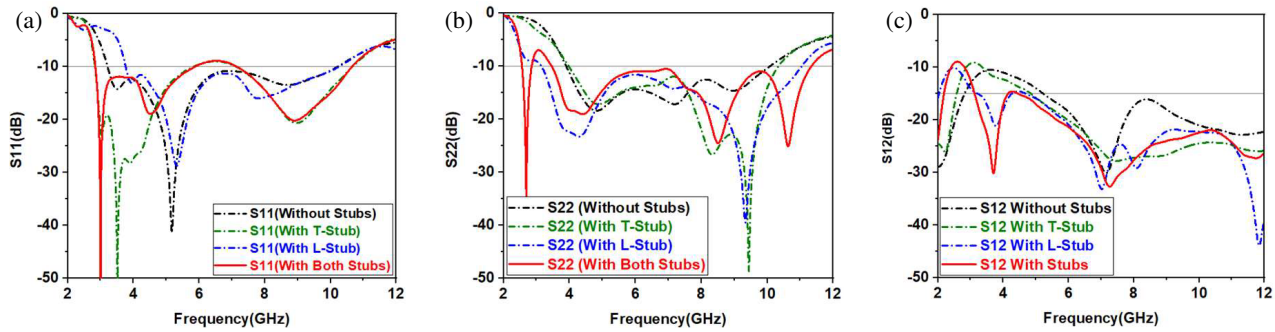

FIGURE 4. S-parameters corresponding to Antenna-3, 4, 5, 6. (a) S_{11}. (b) S_{22}. (c) S_{12}.

ates a resonance near 4 GHz and extends the bandwidth by lowering the cutoff frequency to approximately 2.8 GHz, thereby satisfying UWB criteria. In the case of Antenna-2, the absence of the L-shaped stub results in a lower cutoff frequency close to 4.2 GHz, which is again inadequate for complete UWB operation. The addition of the L-shaped stub, however, generates a resonance at 4.2 GHz and effectively broadens the operating range, enabling coverage from 3.1 GHz to 10.6 GHz.

3.2. UWB MIMO Antenna Evolution (without Notches)

As demonstrated in Fig. 1, the proposed MIMO antenna incorporates a short ground strip linking the two ground planes, together with one T-shaped and L-shaped ground stubs. This configuration significantly contributes to improving both inter-port isolation and impedance performance. The evolutionary stages of the suggested UWB MIMO antenna (Antenna-3, 4, 5, 6) without notch characteristics is demonstrated in Fig. 3. The corresponding S-parameters (S_{11}, S_{22}, and S_{12}) of the aforementioned antennas are depicted in Fig. 4, highlighting the impact of ground stubs through four different cases: without stubs, with only a T-shaped stub, with only an L-shaped stub, and with both stubs included. From Fig. 4(a), it is noted that the presence of only the L-shaped stub produces negligible variation in the impedance bandwidth, as determined by the 10 dB S_{11} criterion, compared to the reference case without stubs. In contrast, the inclusion of the T-shaped stub, either individually or in combination with the L-shaped stub, introduces two distinct resonances around 3.8 GHz and 9 GHz. This will extend the operating band from 3.8–10.1 GHz to 2.9–10.6 GHz.

Figure 4(b) further shows that without stubs, the antenna exhibits resonances near 5 GHz, 7.5 GHz, and 8.5 GHz, resulting in a bandwidth spanning 4–9.5 GHz. When both stubs are employed, four resonance points appear, which broadens the operating range to 2.9–10.6 GHz, and an isolation of $S_{12} < -15$ dB is typically sufficient for reliable MIMO operation. As demonstrated in Fig. 4(c), in the absence of stubs, the isolation bandwidth begins at 5.2 GHz. Incorporating either the L- or T-shaped stub individually provides only marginal improvement, whereas the combined use of both stubs substantially enhances the isolation bandwidth. To further investigate the modal characteristics responsible for these resonances, Characteristic Mode Analysis (CMA) was performed with Multilayer Solver in CST Microwave Studio.

3.2.1. Characteristic Mode Analysis

Characteristic Mode Analysis (CMA) is a systematic approach for investigating the intrinsic electromagnetic behavior of conducting structures. Rather than relying only on port excitation and S-parameters, CMA decomposes the total surface current

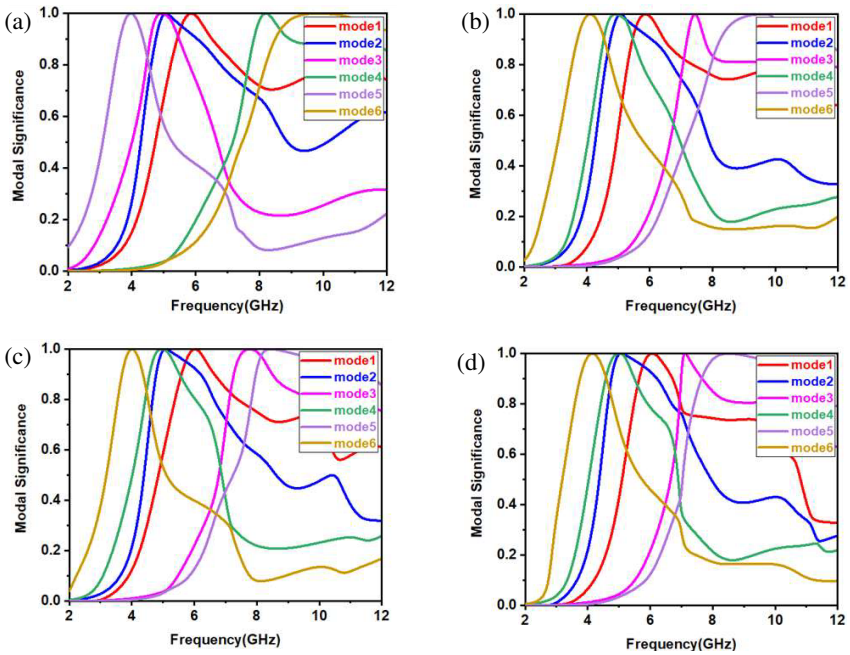

FIGURE 5. (a) Modal significance for Antenna-3. (b) Modal Significance for Antenna-4. (c) Modal significance for Antenna-5. (d) Modal Significance for Antenna-6.

into a set of orthogonal characteristic modes. Each mode is uniquely defined by its eigenvalue, modal significance, characteristic angle, and current distribution. Modal significance (MS) indicates which modes are actively radiating at a given frequency. The MS can be determined from Equation (1).

$$MS = \left| \frac{1}{1 + J\lambda_i} \right| \tag{1}$$

where λ_i represents the eigenvalue of the ith mode. A mode is said to resonate when $\lambda_i = 0$ or equivalently when $MS = 1$. Characteristic angle (CA) is another metric which provides phase based interpretation of how the stored and radiated energies of each mode are balanced. CA is mathematically defined as

$$\alpha_i = 180^0 - \tan^{-1} \lambda_i \tag{2}$$

CMA was further performed for Antenna-3, 4, 5, and 6 to validate their resonant characteristics. MS responses of the first six modes are depicted in Fig. 5. For the configuration without stubs, Modes 2, 3, and 4 are significant within 4–9 GHz, indicating their dominant role in radiation across this frequency region. Since no perturbing structures are present, these modes remain active throughout most of the UWB spectrum. When a T-shaped stub is introduced, the modal behavior changes, with Mode 6 gaining prominence near 4–5 GHz and Mode 2 being suppressed, highlighting the deliberate control of specific resonances. In the case of an L-shaped stub, the modal distribution is altered differently, where Mode 5 becomes dominant in the 8–10 GHz range, while certain lower-order modes, responsible for higher mutual coupling are weakened. With both stubs are employed, a more balanced excitation of modes is achieved in which Modes 3 and 6 dominate in separate frequencies, whereas modes associated with poor isolation are effectively suppressed. These outcomes confirm that the use of ground stubs provides an efficient means to manipulate characteristic modes, enabling selective suppression to optimize UWB-MIMO antenna performance.

3.3. UWB MIMO Antenna for Rejection of Three Narrow Bands

UWB spectrum overlaps with several narrowband standards such as Satellite C-band downlink (3.6–4.6 GHz), WLAN (4.9–5.5 GHz), and Wi-Fi 6E (6.1–6.7 GHz). These coexisting systems can cause electromagnetic interference, which limits the overall system capacity. To mitigate such interference, the integration of band-notched characteristics within UWB antennas has become an effective design approach. The notch bands are designed by adding three U-shaped slots on each radiator.

3.3.1. Designing of Etched Slots

The slot design methodology is demonstrated in Fig. 6(a). The notch bands 3.6–4.6 GHz (centered at 4.33 GHz), 4.9–5.5 GHz (centered at 5.26 GHz), and 6.1–6.7 GHz (centered at 6.61 GHz) are obtained by etching three U-shaped slots on each patch. The length of each U-shaped slot is equal to a quarter wavelength resonator, and the slot length can be calculated as

$$\lambda = \frac{c}{4f\sqrt{\frac{\varepsilon_r + 1}{2}}} \tag{3}$$

where λ is the U-shaped slot length, f various notch frequencies, ε_r the relative permittivity (4.3), and c the speed of light (3×10^{11} mm/s).

Figure 6(b) shows the S_{11} response of the proposed UWB-MIMO antenna with triple band-notched features. The design

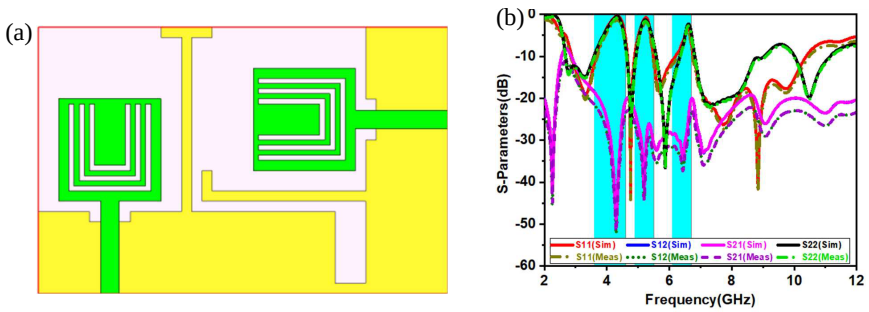

FIGURE 6. (a) Proposed triple band notched UWB MIMO antenna. (b) Simulated and measured S-parameters.

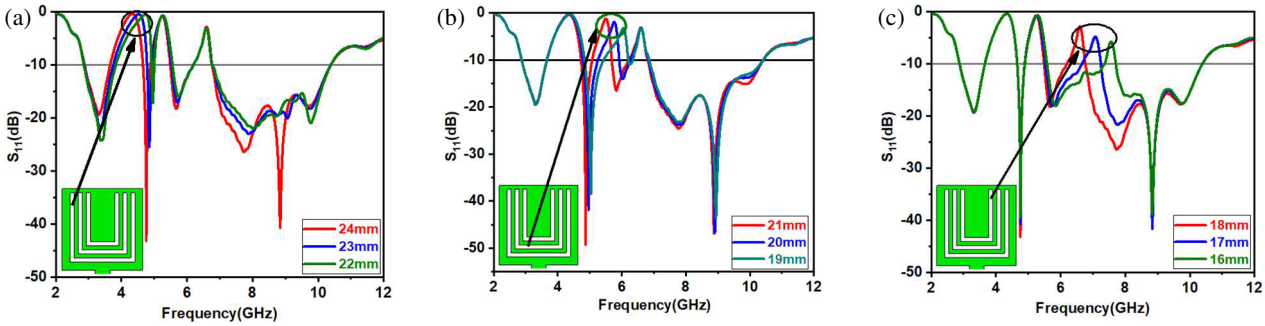

FIGURE 7. Parametric study by varying lengths of (a) Outer U-slot, (b) Middle U-slot, (c) Inner U-slot.

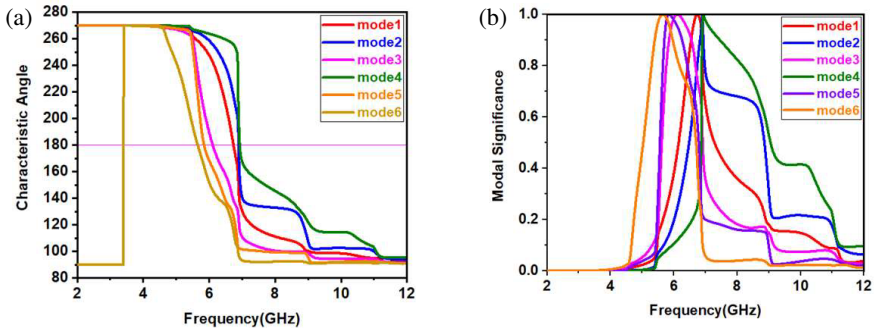

FIGURE 8. Proposed band notched UWB MIMO antenna. (a) Characteristic Angle. (c) Modal significance.

was simulated in CST Microwave Studio and verified using a Vector Network Analyzer (VNA). Distinct notches appear at 4.43 GHz (Satellite C-band), 5.26 GHz (WLAN), and 6.61 GHz (Wi-Fi 6E). The antenna achieves an impedance bandwidth of 2.9–10.6 GHz with isolation better than -20 dB, and simulation results agree well with measurements.

The impact of slot length on the notched frequencies was analyzed through parametric analysis, as illustrated in Figs. 7(a), 7(b), and 7(c). The results indicate that longer slots shift the stopband toward lower frequencies, while shorter slots push the notch to higher frequencies, allowing accurate tuning of the triple-band rejection.

While S-parameters effectively illustrate impedance behavior, they do not directly explain the underlying radiation and suppression mechanisms. To address this, Characteristic Mode Analysis (CMA) was applied to the proposed band notched UWB-MIMO antenna, and the results were correlated with S_{11} characteristics. At 4.33 GHz, peak of the notch frequency coincides with a CA deviation from the resonance value of 180° and a suppressed MS (< 0.707) for the dominant lower-order mode, as illustrated in Figs. 8(a)–8(b).

The 5.26 GHz notch originates from the deviation of CA from resonance, and MS falls below the radiation threshold, thereby weakening radiation in the WLAN band. Similarly, the 6.61 GHz notch arises from the suppression of Mode-3 and Mode-4, reflected by a sharp MS drop and a non-resonant CA. In contrast, in the passbands, dominant modes maintain $MS = 1$, enabling strong and effective radiation. The interpretations drawn from CA and MS characteristics are further confirmed by the modal current distributions and radiation patterns of the dominant modes at the notched frequencies, as depicted in Fig. 9. At 4.33 GHz, strong current localization around the outer U-shaped slot introduces destructive interference with radiator currents, suppressing Mode-5 and producing distorted far-field radiation with deep rejection in S_{11}. At 5.26 GHz, currents are confined to the middle slot, suppressing Mode-4 and

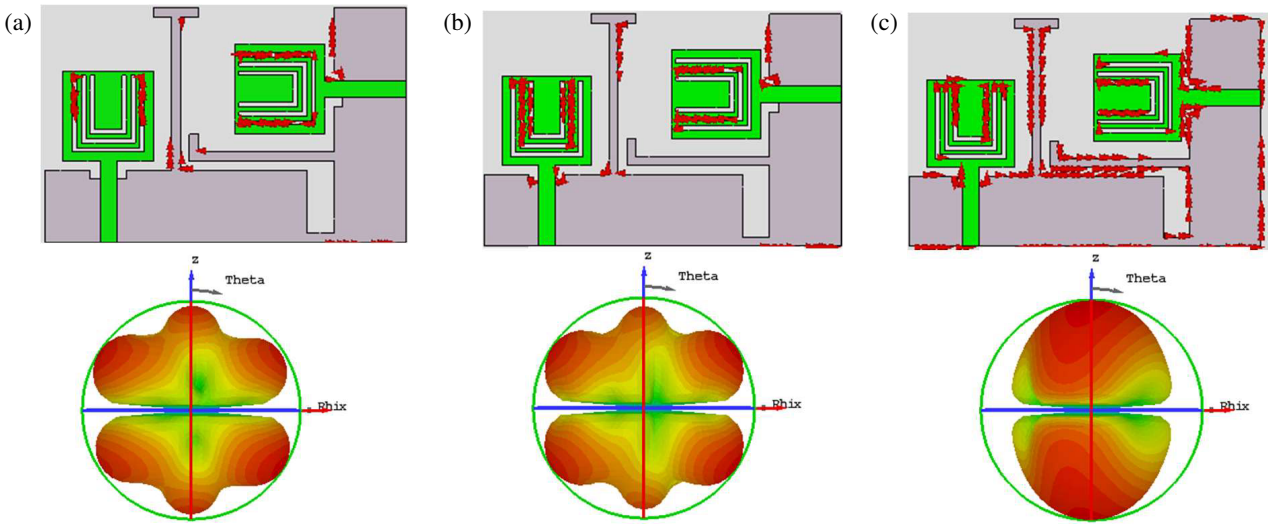

FIGURE 9. Modal currents and modal patterns of proposed antenna at notch frequencies. (a) 4.33 GHz. (b) 5.26 GHz. (c) 6.61 GHz.

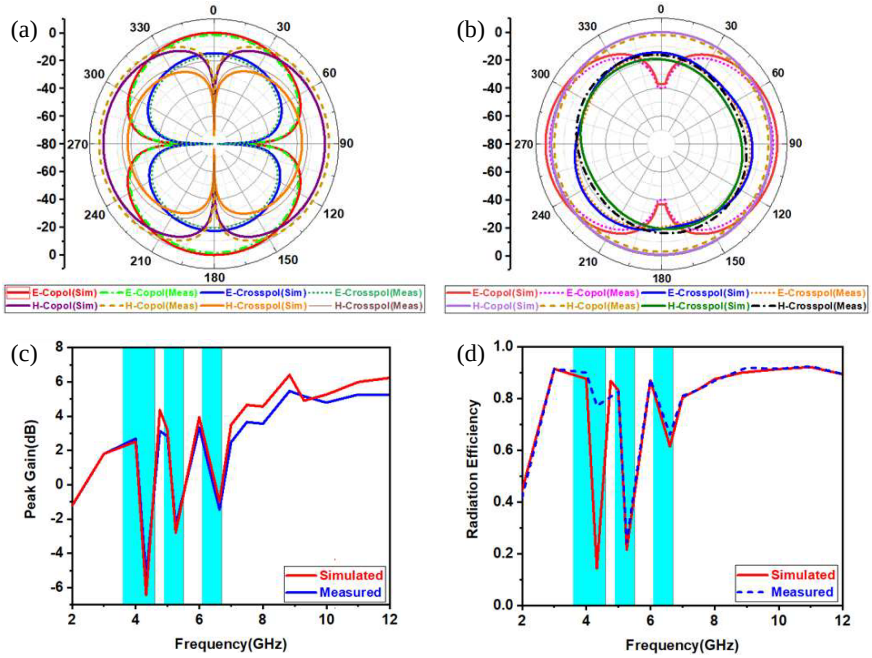

FIGURE 10. Radiation patterns at resonant frequencies. (a) 4.76 GHz. (b) 8.84 GHz. (c) Gain. (d) Radiation Efficiency.

leading to minimal radiation in the WLAN band. At 6.61 GHz, the notching elements perturb the radiator edge currents, suppressing Mode-4, resulting in negligible far-field contribution. These observations confirm that the triple notches are realized through selective mode suppression.

4. RESULTS AND DISCUSSION

4.1. Radiation Performance

Figures 10(a) & (b) demonstrate the simulated and measured radiation patterns of the proposed UWB MIMO antenna at 4.76 GHz and 8.84 GHz (outside notch bands), with co and cross polarization responses in E- & H-planes. At both frequencies, the antenna demonstrates omnidirectional radiation in H-plane, whereas the E-plane shows a broad boresight directed main lobe.

Figures 10(c) and 10(d) show the peak gain and radiation efficiency of the proposed antenna. The antenna maintains stable gain and over 90% efficiency across the passband, while at the notched frequencies (4.43, 5.26, and 6.61 GHz), the gain drops below 0 dB, and efficiency falls under 50%, thereby validating the effectiveness of the U-shaped slots in achieving selective band rejection.

4.2. Surface Current Distribution

Figure 11 depicts the surface current distributions at three notched frequencies (4.43 GHz, 5.26 GHz, and 6.61 GHz) for port-1 and port-2 excitation. Strong localization of currents is

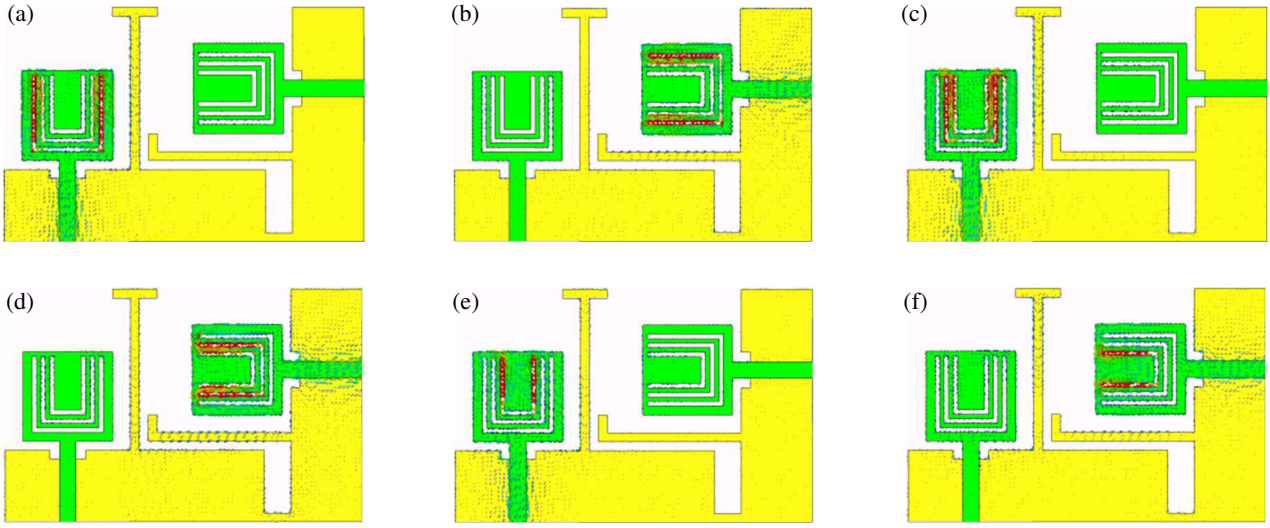

FIGURE 11. Surface current distribution. (a) Port-1 excited (4.43 GHz). (b) Port-2 excited (4.43 GHz). (c) Port-1 excited (5.26 GHz). (d) Port-2 excited (5.26 GHz). (e) Port-1 excited (6.61 GHz). (f) Port-2 excited (6.61 GHz).

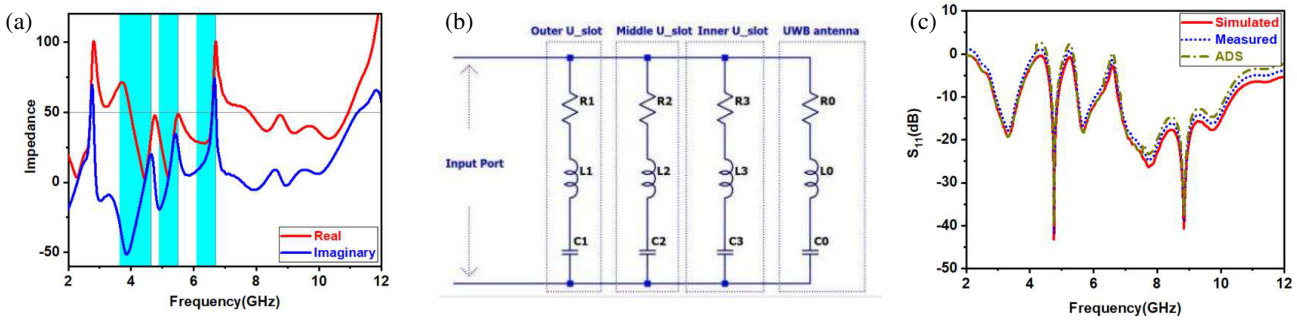

FIGURE 12. (a) Impedance versus frequency. (b) RLC equivalent circuit. (c) S_{11}.

TABLE 2. Calculated R, L, C values.

	BW (GHz)	Q_0	R in Ω	L in nH	C in pF
UWB Antenna	3–12	-	50	0.147	10.2
First notch (4.43 GHZ)	1	4.43	10	1.59	0.811
Second notch (5.26 GHZ)	0.6	8.76	10	0.303	3.02
Third notch (6.61 GHZ)	0.6	11	21	0.51	1.14

observed on the outer, middle, and inner U-shaped slots at 4.43, 5.26, and 6.61 GHz, respectively.

4.3. Equivalent Circuit Analysis

An equivalent circuit is developed to characterize the band notching behavior. As demonstrated in Fig. 12(a), the input impedance exhibits series resonance at 4.43, 5.26, and 6.61 GHz, where the real part approaches 50 Ω, and the imaginary part changes slope from negative to positive. The extracted RLC parameters and quality factor Q_0, calculated from Equations (4)–(6), are summarized in Table 2.

$$f_{notch,i} = \frac{1}{2\pi\sqrt{L_i C_i}} \tag{4}$$

$$Q_0 = \frac{1}{2\pi f_{notch,i} R_i C_i} \tag{5}$$

$$BW = \frac{f_{notch,i}}{Q_0} \tag{6}$$

Using Advanced Design System (ADS), the antenna is modeled with an RLC network and is demonstrated in Fig. 12(b). Fig. 12(c) compares the impedance response of the circuit model with CST simulations, showing close agreement.

4.4. Diversity Performance

The diversity performance of the suggested band-notched UWB MIMO antenna has been comprehensively evaluated

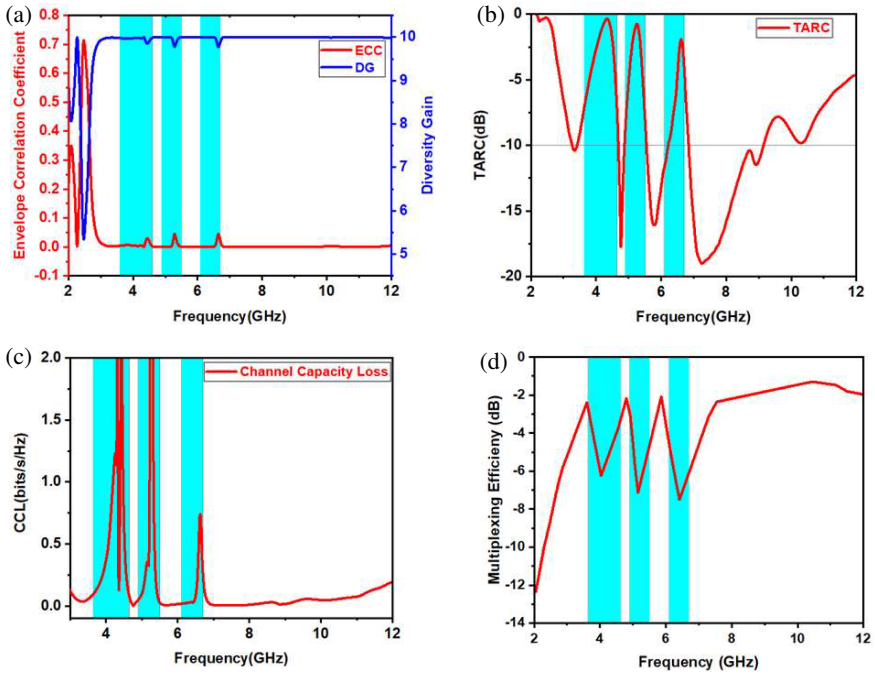

FIGURE 13. (a) ECC and DG. (b) TARC. (c) CCL. (d) Multiplexing efficiency.

using several standard metrics, including Envelope Correlation Coefficient (ECC), Diversity Gain (DG), Total Active Reflection Coefficient (TARC), Channel Capacity Loss (CCL), Multiplexing Efficiency, and Group Delay.

4.4.1. Envelope Correlation Coefficient and Diversity Gain

Figure 13(a) depicts the frequency dependent variation of ECC and DG. Lower ECC value indicates lower correlation and thus better diversity gain. The suggested antenna exhibits $ECC < 0.02$ and $DG = 10$ dB across the passbands, indicating highly uncorrelated radiation patterns and near-ideal diversity performance. ECC and DG can be calculated from

$$ECC = \frac{\left|S_{ii} * S_{ij} + S_{ji} * S_{jj}\right|^2}{\left(1 - \left|S_{ii}\right|^2 - S_{ij}^2\right)\left(1 - \left|S_{ji}\right|^2 - S_{jj}^2\right)} \quad (7)$$

$$DG = 10\sqrt{1 - ECC^2} \quad (8)$$

4.4.2. Total Active Reflection Coefficient

TARC evaluates the performance of MIMO antenna under simultaneous excitation at all ports. $TARC < -10$ dB indicates better impedance matching and reduced mutual coupling. TARC can be calculated as

$$TARC = \sqrt{\frac{\left|S_{11} + S_{12}\right|^2 + \left|S_{21} + S_{22}^2\right|}{2}} \quad (9)$$

The suggested antenna maintains TARC less than -10 dB in passbands, while sharp peaks near 0 dB at 4.43, 5.26, and 6.61 GHz validate effective notch operation as demonstrated in Fig. 13(b).

4.4.3. Channel Capacity Loss

CCL quantifies the reduction in the maximum achievable data rate of a MIMO system due to mutual coupling. CCL remains well below the 0.4 bits/s/Hz limit in passbands, ensuring minimal channel capacity degradation, but rises to 1.41–1.85 bits/s/Hz at the notches due to intentional signal suppression as depicted in Fig. 13(c). CCL is expressed as

$$CCL = -\log_2 \det\left|\psi^R\right| \quad (10)$$

4.4.4. Multiplexing Efficiency

Multiplexing efficiency accounts for both the radiation efficiency of individual elements and the correlation between them. Fig. 13(d) depicts the multiplexing efficiency versus frequency for the proposed antenna. Multiplexing efficiency stays close to 0 dB in passbands and drops to -9.7 to -11.5 dB in rejection bands, reflecting the designed isolation.

$$\eta_{mux} = \sqrt{\eta_i \eta_j \left(1 - \left|\rho_c\right|^2\right)} \quad (11)$$

4.4.5. Group Delay

The group delay of the suggested triple band notched UWB MIMO antenna was evaluated for face-to-face and side-by-side configurations. In both cases, a nearly constant delay is maintained across the passband (± 0.2 ns), ensuring dispersion-free transmission. The face-to-face setup yields 0.4–0.6 ns, while the side-by-side arrangement shows 0.6–0.8 ns due to stronger coupling which is depicted in Figs. 14(a) and 14(b). Fig. 14(c) depicts the fabricated prototype antenna inside an anechoic

TABLE 3. Comparison with existing designs

Ref.	Size (mm^2)	BW (GHz)	No. of notches	Isolation (dB)	ECC	DG (dB)	TARC (dB)	Multiplexing Efficiency	CCL (bits/s/Hz)
[11]	45×45	2–10.6	1	-17	< 0.005	-	-	-	< 0.3
[17]	34×17	3.06–12.92	4	-17	< 0.016	> 9.92	< -8	-	< 0.1
[18]	38×38	3.3–10	1	-20	< 0.0006	> 9.99	-	-	< -10
[19]	40×21	2.94–11.61	1	-18	< 0.002	> 9.99	-	-	-
[25]	50×82	2.2–13.35	1	-15	< 0.04	> 9.99	-	< -1	-
[26]	18×36	2.2–20	1	-20	< 0.012	> 9.95	-	< -0.6	-
[27]	35×68	3.1–10.6	2	-20	< 0.002	-	-	-	-
[28]	30×22	3.1–10.6	1	-15	< 0.05	-	-	-	-
[29]	22×36	3.1–11	1	-15	< 0.1	-	-	-1	-
[30]	41×41	2.95–10.65	2	-16	< 0.15	-	-	-	< 0.4
[31]	48×48	2.5–12	1	-15	< 0.005	-	-	-	-
Prop.	**25×39**	**2.9–10.6**	**3**	**-20**	**< 0.02**	**> 9.99**	**< -10**	**< -1**	**< 0.4**

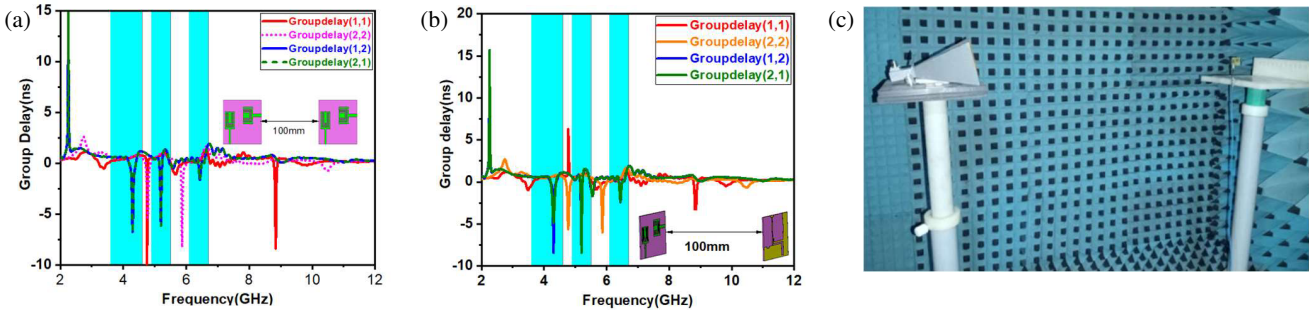

FIGURE 14. Group delay. (a) Side by side. (b) Face to face. (c) Measurement inside anechoic chamber.

chamber. A comparative performance summary with previously published designs are presented in Table 3.

5. CONCLUSION

A compact dual-port UWB MIMO antenna with triple band rejection has been designed and validated for portable wireless applications. Orthogonal element placement with T- and L-shaped ground stubs provides wide impedance bandwidth and high isolation, while three U-shaped slots suppress Satellite C-band, WLAN, and Wi-Fi 6E interference. Characteristic Mode Analysis explains the modal behavior and notch formation. Simulated and measured results confirm stable operation over 2.9–10.6 GHz, achieving 90% efficiency, 6.2 dBi peak gain, isolation better than -20 dB, and ECC < 0.02. Diversity metrics (DG, TARC, CCL, multiplexing efficiency) further demonstrate robustness in multipath environments. The design can be extended for reconfigurable band-notching using PIN diodes/varactors, integration with 5G/6G frequency bands, and optimization for wearable or IoT devices.

REFERENCES

[1] Alsath, M. G. N. and M. Kanagasabai, "Compact UWB monopole antenna for automotive communications," *IEEE Transactions on Antennas and Propagation*, Vol. 63, No. 9, 4204–4208, Sep. 2015.

[2] Staderini, E. M., "UWB radars in medicine," *IEEE Aerospace and Electronic Systems Magazine*, Vol. 17, No. 1, 13–18, Jan. 2002.

[3] Kshetrimayum, R. S., "An introduction to UWB communication systems," *IEEE Potentials*, Vol. 28, No. 2, 9–13, Mar.–Apr. 2009.

[4] Sharma, N. and S. S. Bhatia, "Design of printed UWB antenna with CPW and microstrip-line-fed for DCS/PCS/bluetooth/WLAN wireless applications," *International Journal of RF and Microwave Computer-Aided Engineering*, Vol. 31, No. 1, e22488, 2020.

[5] Tiwari, R. N., P. Singh, and B. K. Kanaujia, "A modified microstrip line fed compact UWB antenna for WiMAX/ISM/WLAN and wireless communications," *AEU — International Journal of Electronics and Communications*, Vol. 104, 58–65, May 2019.

[6] Kumari, E. K., J. R. Szymanski, M. Zurek-Mortka, and M. Sathiyanarayanan, "Design and development of compact UWB-MIMO antenna with enhanced isolation for short distance V2X communications," *Journal of Electromagnetic Waves and Applications*, 1–24, 2025.

[7] Zhang, S. and G. F. Pedersen, "Mutual coupling reduction for UWB MIMO antennas with a wideband neutralization line," *IEEE Antennas and Wireless Propagation Letters*, Vol. 15, 166–169, 2016.

[8] Wang, H., D. G. Fang, and X. L. Wang, "Mutual coupling reduction between two microstrip patch antennas by using the parasitic elements," in *2008 Asia-Pacific Microwave Conference*, 1–4, Hong Kong, China, 2008.

[9] Acharjee, J., K. Mandal, and S. K. Mandal, "Reduction of mutual coupling and cross-polarization of a MIMO/diversity antenna using a string of H-shaped DGS," *AEU — International Journal of Electronics and Communications*, Vol. 97, 110–119, 2018.

[10] Zhu, J., S. Li, B. Feng, L. Deng, and S. Yin, "Compact dual-polarized UWB quasi-self-complementary MIMO/diversity antenna with band-rejection capability," *IEEE Antennas and Wireless Propagation Letters*, Vol. 15, 905–908, 2016.

[11] Tripathi, S., A. Mohan, and S. Yadav, "A compact Koch fractal UWB MIMO antenna with WLAN band-rejection," *IEEE Antennas and Wireless Propagation Letters*, Vol. 14, 1565–1568, 2015.

[12] Khan, M. S., A. D. Capobianco, S. Asif, A. Iftikhar, B. Ijaz, and B. D. Braaten, "Compact 4 × 4 UWB-MIMO antenna with WLAN band rejected operation," *Electronics Letters*, Vol. 51, No. 14, 1048–1050, 2015.

[13] Biswal, S. P. and S. Das, "A low-profile dual port UWB-MIMO/diversity antenna with band rejection ability," *International Journal of RF and Microwave Computer-Aided Engineering*, Vol. 28, No. 1, e21159, 2017.

[14] Li, Z., C. Yin, and X. Zhu, "Compact UWB MIMO Vivaldi antenna with dual band-notched characteristics," *IEEE Access*, Vol. 7, 38 696–38 701, 2019.

[15] Kumar, A., A. Q. Ansari, B. K. Kanaujia, J. Kishor, and S. Kumar, "An ultra-compact two-port UWB-MIMO antenna with dual band-notched characteristics," *AEU — International Journal of Electronics and Communications*, Vol. 114, 152997, 2020.

[16] Kadam, A. A. and A. A. Deshmukh, "Pentagonal shaped UWB antenna loaded with slot and EBG structure for dual band notched response," *Progress In Electromagnetics Research M*, Vol. 95, 165–176, 2020.

[17] Pannu, P., "Highly compact UWB-MIMO antenna with sharp multi-stop band characteristics," *EURASIP Journal on Wireless Communications and Networking*, Vol. 2024, No. 1, 48, 2024.

[18] Dalakoti, N. and P. Jain, "A compact dual-element UWB-MIMO antenna with single band-notched characteristics," *Frequenz*, Vol. 78, No. 7-8, 335–345, 2024.

[19] Devana, V. N. K. R., A. Beno, C. P. Devadoss, Y. Sukanya, C. V. R. Sankar, P. Balamuralikrishna, S. Chandrasekhar, and K. V. Babu, "A compact self isolated MIMO UWB antenna with band notched characteristics," *IETE Journal of Research*, Vol. 70, No. 8, 6677–6688, 2024.

[20] Chen, Z., W. Zhou, and J. Hong, "A miniaturized MIMO antenna with triple band-notched characteristics for UWB applications," *IEEE Access*, Vol. 9, 63 646–63 655, 2021.

[21] Kumar, P., S. Urooj, and F. Alrowais, "Design of quad-port MIMO/Diversity antenna with triple-band elimination characteristics for super-wideband applications," *Sensors*, Vol. 20, No. 3, 624, 2020.

[22] Jayant, S. and G. Srivastava, "Close-packed quad-element triple-band-notched UWB MIMO antenna with upgrading capability," *IEEE Transactions on Antennas and Propagation*, Vol. 71, No. 1, 353–360, Jan. 2023.

[23] Kumar, P., T. Ali, and M. P. Mm, "Characteristic mode analysis-based compact dual band-notched UWB MIMO antenna loaded with neutralization line," *Micromachines*, Vol. 13, No. 10, 1599, 2022.

[24] Mukherjee, S., A. Roy, S. Maity, T. Tewary, P. P. Sarkar, and S. Bhunia, "Design of dual band-notched UWB hexagonal printed microstrip antenna," *International Journal of Microwave and Wireless Technologies*, Vol. 15, No. 3, 526–534, 2023.

[25] Toktas, A., "G-shaped band-notched ultra-wideband MIMO antenna system for mobile terminals," *IET Microwaves, Antennas & Propagation*, Vol. 11, No. 5, 718–725, 2017.

[26] Chandel, R. and A. K. Gautam, "Compact MIMO/diversity slot antenna for UWB applications with band-notched characteristic," *Electronics Letters*, Vol. 52, No. 5, 336–338, 2016.

[27] Li, W. T., Y. Q. Hei, H. Subbaraman, X. W. Shi, and R. T. Chen, "Novel printed filtenna with dual notches and good out-of-band characteristics for UWB-MIMO applications," *IEEE Microwave and Wireless Components Letters*, Vol. 26, No. 10, 765–767, 2016.

[28] Tao, J. and Q. Feng, "Compact UWB band-notch MIMO antenna with embedded antenna element for improved band notch filtering," *Progress In Electromagnetics Research C*, Vol. 67, 117–125, 2016.

[29] Liu, L., S. W. Cheung, and T. I. Yuk, "Compact MIMO antenna for portable UWB applications with band-notched characteristic," *IEEE Transactions on Antennas and Propagation*, Vol. 63, No. 5, 1917–1924, May 2015.

[30] Srivastava, G. and B. K. Kanuijia, "Compact dual band-notched UWB MIMO antenna with shared radiator," *Microwave and Optical Technology Letters*, Vol. 57, No. 12, 2886–2891, 2015.

[31] Gao, P., S. He, X. Wei, Z. Xu, N. Wang, and Y. Zheng, "Compact printed UWB diversity slot antenna with 5.5-GHz band-notched characteristics," *IEEE Antennas and Wireless Propagation Letters*, Vol. 13, 376–379, 2014.

[32] Garbacz, R. J., "Modal expansions for resonance scattering phenomena," *Proceedings of the IEEE*, Vol. 53, No. 8, 856–864, Aug. 1965.